Dynamics of Colombo's Top: Tidal Dissipation and Resonance Capture

Yubo Su,[1★], Dong Lai[1,2]
[1] Cornell Center for Astrophysics and Planetary Science, Department of Astronomy, Cornell University, Ithaca, NY 14853, USA
[2] Tsung-Dao Lee Institute & School of Physics and Astronomy, Shanghai Jiao Tong University, 200240 Shanghai, China

Accepted XXX. Received YYY; in original form ZZZ

ABSTRACT
Abstract here

Key words: planet-star interactions

1 INTRODUCTION

- Studying planetary obliquities (define) is important. Cassini States are key. More introduction.
- Resonance capture via separatrix crossing was first considered by (Henrard 1982) for non-dissipative perturbations (e.g. Su & Lai 2020). However, tidal friction is dissipative, so this formalism does not apply. We generalize this calculation and show that it reproduces results.

In Section XXX...

2 SPIN EVOLUTION EQUATIONS AND CASSINI STATES: REVIEW

In this section, we first briefly lay out the spin dynamics of the planet, introducing the Cassini State spin-orbit resonance (for more details, see Su & Lai 2020). We then introduce the weak friction theory of equilibrium tides used in this work (Lai 2012). While many different tidal effects may dominate in different planetary systems, our qualitative conclusions do not depend on the specific form of the tidal dissipation, so we use the classic weak friction theory for simplicity.

2.1 Spin Dynamics in the Absence of Tides

2.1.1 Equations of Motion

We consider a star of mass $M_\star$ hosting an inner oblate planet of mass m and radius R on a circular orbit with semi-major axis a and an outer perturber of mass $m_{\rm p}$ on a circular orbit with semi-major axis $a_{\rm p}$. We assume that the two orbits are mildly misaligned with mutual inclination I. Denote $\mathbf{S}$ the spin angular momentum and $\mathbf{L}$ the orbital angular momentum of the planet, and $\mathbf{L}_{\rm p}$ the angular momentum of the perturber. The corresponding unit vectors are $\hat{\mathbf{s}} \equiv \mathbf{S}/S$, $\hat{\mathbf{l}} \equiv \mathbf{L}/L$, and $\hat{\mathbf{l}}_{\rm p} \equiv \mathbf{L}_{\rm p}/L_{\rm p}$. The spin axis $\hat{\mathbf{s}}$ of the planet tends to precess around its orbital (angular momentum) axis $\hat{\mathbf{l}}$, driven by the gravitational torque from the host star acting on the planet's rotational bulge. On the other hand, $\hat{\mathbf{l}}$ and the disk axis $\hat{\mathbf{l}}_{\rm p}$ precess around each other due to gravitational interactions. We assume $S \ll L \ll L_{\rm p}$, so $\hat{\mathbf{l}}_{\rm p}$ and $\hat{\mathbf{l}}$ are nearly constant. The equations of motion for $\hat{\mathbf{s}}$ and $\hat{\mathbf{l}}$ in this limit are (Anderson & Lai 2018; Su & Lai 2020)

$$\frac{\mathrm{d}\hat{\mathbf{s}}}{\mathrm{d}t} = \omega_{\rm sl}\left(\hat{\mathbf{s}}\cdot\hat{\mathbf{l}}\right)\left(\hat{\mathbf{s}}\times\hat{\mathbf{l}}\right) \equiv \alpha\left(\hat{\mathbf{s}}\cdot\hat{\mathbf{l}}\right)\left(\hat{\mathbf{s}}\times\hat{\mathbf{l}}\right), \tag{1}$$

$$\frac{\mathrm{d}\hat{\mathbf{l}}}{\mathrm{d}t} = \omega_{\rm lp}\left(\hat{\mathbf{l}}\cdot\hat{\mathbf{l}}_{\rm p}\right)\left(\hat{\mathbf{l}}\times\hat{\mathbf{l}}_{\rm p}\right) \equiv -g\left(\hat{\mathbf{l}}\times\hat{\mathbf{l}}_{\rm p}\right), \tag{2}$$

where

$$\omega_{\rm sl} \equiv \frac{3GJ_2 mR^2 M_\star}{2a^3 I\Omega_{\rm s}} = \frac{3k_q}{2k}\frac{M_\star}{m}\left(\frac{R}{a}\right)^3\Omega_{\rm s}, \tag{3}$$

$$\omega_{\rm lp} = \frac{3m_p}{4M_\star}\left(\frac{a}{a_{\rm p}}\right)^3 n. \tag{4}$$

In Eq. (3), $\Omega_{\rm s}$ is the spin frequency of the inner planet, $I = kmR^2$ (with k a constant) is its moment of inertia and $J_2 = k_{\rm q}\Omega_{\rm s}^2(R^3/Gm)$ (with k_q a constant) is its rotation-induced (dimensionless) quadrupole moment [for a body with uniform density, $k = 0.4, k_{\rm q} = 0.5$; for rocky planets, $k \simeq 0.2$ and $k_{\rm q} \simeq 0.17$ (e.g. Lainey 2016) ? not sure]. In other studies, $3k_{\rm q}/2k$ is often notated as $k_2/2C$ (e.g. Millholland & Batygin 2019). In Eq. (4), $n \equiv \sqrt{GM_\star/a^3}$ is the inner planet's orbital mean motion, and we have assumed $a_{\rm p} \gg a$ and included only the leading-order (quadrupole) interaction between the inner planet and perturber. Following standard notation, we define $\alpha = \omega_{\rm sl}$ and $g \equiv -\omega_{\rm lp}\cos I$ (e.g. Colombo 1966).

As in Su & Lai (2020), we combine Eqs. (1–2) into a single equation by transforming into a frame rotating about $\hat{\mathbf{l}}_{\rm p}$ with frequency g. In this frame, $\hat{\mathbf{l}}_{\rm p}$ and $\hat{\mathbf{l}}$ are both fixed, and $\hat{\mathbf{s}}$ evolves as:

$$\left(\frac{\mathrm{d}\hat{\mathbf{s}}}{\mathrm{d}t}\right)_{\rm rot} = \alpha\left(\hat{\mathbf{s}}\cdot\hat{\mathbf{l}}\right)\left(\hat{\mathbf{s}}\times\hat{\mathbf{l}}\right) + g\left(\hat{\mathbf{s}}\times\hat{\mathbf{l}}_{\rm p}\right). \tag{5}$$

In this reference frame, we choose the coordinate system such that $\hat{\mathbf{z}} = \hat{\mathbf{l}}$ and $\hat{\mathbf{l}}_{\rm p}$ lies in the $\hat{\mathbf{x}}$-$\hat{\mathbf{z}}$ plane. We describe $\hat{\mathbf{s}}$ in spherical coordinates using the polar angle θ, the planet's obliquity, and ϕ, the precessional phase of $\hat{\mathbf{s}}$ about $\hat{\mathbf{l}}$.

The equilibria of Eq. (5) are referred to as *Cassini States* (CSs; Colombo 1966; Peale 1969). We follow the notation of Su & Lai (2020), where the parameter

$$\eta \equiv -\frac{g}{\alpha}, \tag{6}$$

is used. For a given value of η, there can be either two or four CSs, all of which require $\hat{\mathbf{s}}$ lie in the plane of $\hat{\mathbf{l}}$ and $\hat{\mathbf{l}}_{\rm p}$. Following the standard

★ E-mail: yubosu@astro.cornell.edu

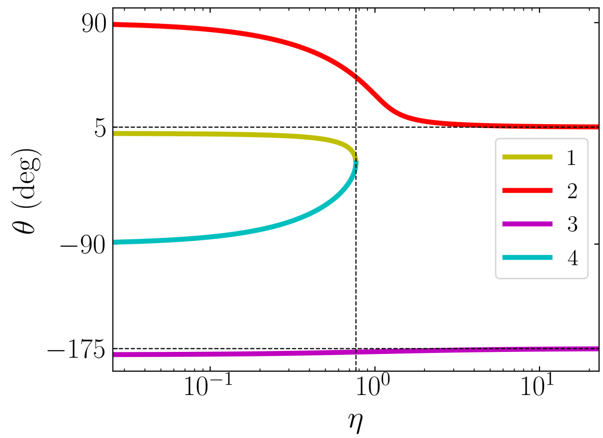

Figure 1. Cassini State obliquities θ as a function of $\eta \equiv -g/\alpha$ (Eq. 6) for $I = 5°$. The vertical dashed line denotes η_c, where the number of Cassini States changes from four to just two (Eq. 8). The horizontal dashed line gives $\theta = I$, the asymptotic value of Cassini State 2's obliquity when $\eta \to \infty$.

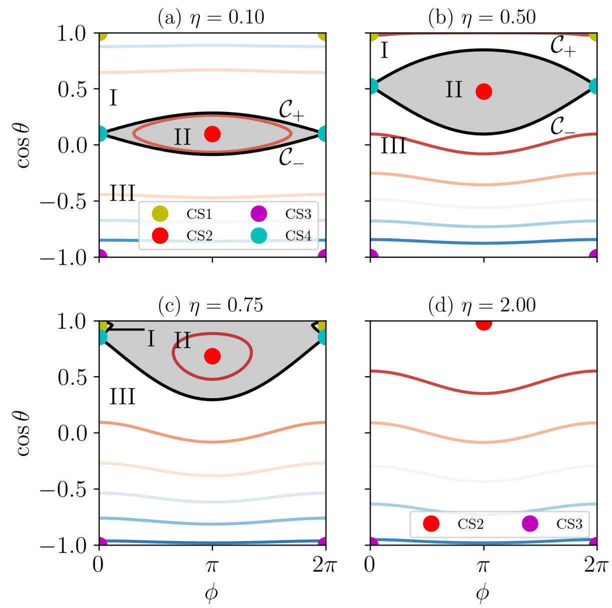

Figure 2. Level curves of the Cassini State Hamiltonian (Eq. 9) for $I = 5°$, for which $\eta_c \approx 0.77$ (Eq. 8). For $\eta < \eta_c$, there are four Cassini States (labeled), while for $\eta > \eta_c$ there are only two. In the former case, the existence of a *separatrix* (solid black lines) separates phase space into three numbered zones (I/II/III, labeled). Finally, we denote the upper and lower legs of the separatrix by $\mathcal{C}_\pm$ respectively, as shown in the upper two panels.

convention and nomenclature, CSs 1, 3, and 4 have $\phi = 0$ and $\theta < 0$, while CS2 has $\phi = \pi$ and $\theta > 0$. Figure 1 shows the CS obliquities as a function of η, each of which satisfies

$$\sin\theta\cos\theta - \eta\sin(\theta - I) = 0. \tag{7}$$

Note that there are four CSs when $\eta < \eta_c$ and only two when $\eta > \eta_c$, where

$$\eta_c \equiv \left(\sin^{2/3} I + \cos^{2/3} I\right)^{-3/2}. \tag{8}$$

The Hamiltonian corresponding to Eq. (5) is

$$\begin{aligned} H &= -\frac{\alpha}{2}\left(\hat{\mathbf{s}} \cdot \hat{\mathbf{l}}\right)^2 - g\left(\hat{\mathbf{s}} \cdot \hat{\mathbf{l}}_{\rm d}\right) \\ &= -\frac{\alpha}{2}\cos^2\theta - g\left(\cos\theta\cos I - \sin I\sin\theta\cos\phi\right). \end{aligned} \tag{9}$$

Here, $\cos\theta$ and ϕ form a canonically conjugate pair of variables. Figure 2 shows the level curves of this Hamiltonian for $I = 20°$, for which $\eta_c \approx 0.77$ (Eq. 8). When $\eta < \eta_c$, CS4 exists and is a saddle point. The two trajectories originating and ending at CS4 are the only two infinite-period orbits in the phase space. Together, these two critical trajectories are referred to as the *separatrix* and divide phase space into three zones. Trajectories in zone II librate about CS2 while those in zones I and III circulate. On the other hand, when $\eta > \eta_c$, all trajectories circulate. When the separatrix exists, we divide it into two curves: $\mathcal{C}_+$, the boundary between zones I and II, and $\mathcal{C}_-$, the boundary between zones II and III.

3 SPIN EVOLUTION WITH ALIGNMENT TORQUE

In this section, we consider a simplified model of equilibrium tides that isolates the important new phenomenon presented in this paper. We assume that the spin magnitude of the planet is constant, so α and g are both fixed, while the spin orientation $\hat{\mathbf{s}}$ experiences an alignment torque towards $\hat{\mathbf{l}}$ on the alignment timescale t_s:

$$\left(\frac{\mathrm{d}\hat{\mathbf{s}}}{\mathrm{d}t}\right)_{\rm tide} = \frac{1}{t_s}\hat{\mathbf{s}} \times \left(\hat{\mathbf{l}} \times \hat{\mathbf{s}}\right). \tag{10}$$

The full equations of motion for $\hat{\mathbf{s}}$ in the coordinates θ and ϕ can be written:

$$\frac{\mathrm{d}\theta}{\mathrm{d}t} = -g\sin I\sin\phi - \frac{1}{t_s}\sin\theta, \tag{11}$$

$$\frac{\mathrm{d}\phi}{\mathrm{d}t} = -\alpha\cos\theta - g\left(\cos I + \sin I\cot\theta\cos\phi\right). \tag{12}$$

3.1 Shifted Cassini States and Linear Stability Analysis

If the alignment torque is weak ($|gt_s| \gg 1$), then the fixed points of Eqs. (11–12) are just slightly shifted CSs. This shift can be calculated cleanly to leading order: all of the CS obliquities $\theta_{\rm cs}$ are unchanged while the azimuthal angle $\phi_{\rm cs}$ for each CS now satisfies

$$\sin\phi_{\rm cs} = \frac{\sin\theta_{\rm cs}}{\sin I\,|g|\,t_s}. \tag{13}$$

We can see that if $t_s > t_{s,c}$, where

$$t_{s,c} = \frac{1}{|g|\sin I}, \tag{14}$$

then Eq. (13) will always have solutions for $\phi_{\rm cs}$, and the alignment torque never changes the number of fixed points of the system. If t_s is decreased below $t_{s,c}$, CS2 and CS4 cease to be fixed points if $\eta \ll 1$ (as first noted in Fabrycky et al. 2007), as $\theta_{\rm cs} \approx 90°$ for these (see Fig. 1), while the other CSs have small $\sin\theta_{\rm cs}$ and are only slightly perturbed. Figure 3 shows the obliquity and azimuthal angles for each of the CSs in the $\eta \ll 1$ case, where it can be seen that CS2 and CS4 collide and annihilate.. For the remainder of this section, we will consider the case where $t_s \gg t_{s,c}$ and the CSs only differ slightly from their unperturbed locations.

We next seek to characterize the stability of small perturbations

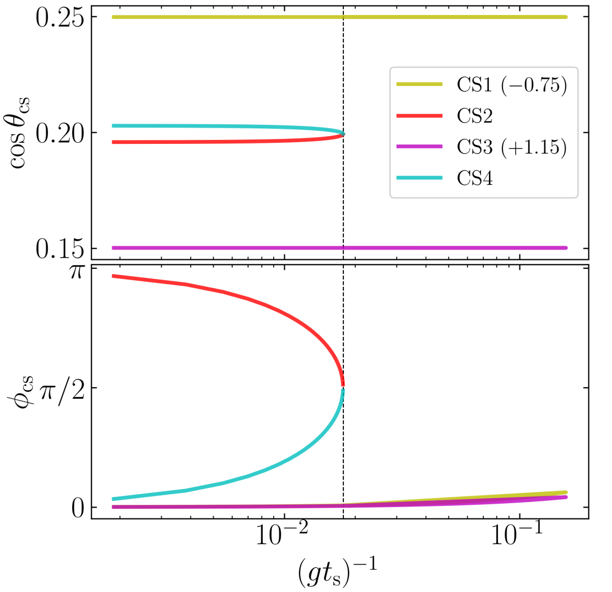

Figure 3. Modified CSs for $I = 5°$ and $\eta = 0.2$, and the CS1 and CS3 obliquities have been offset (labeled in legend) to improve clarity of the plot.

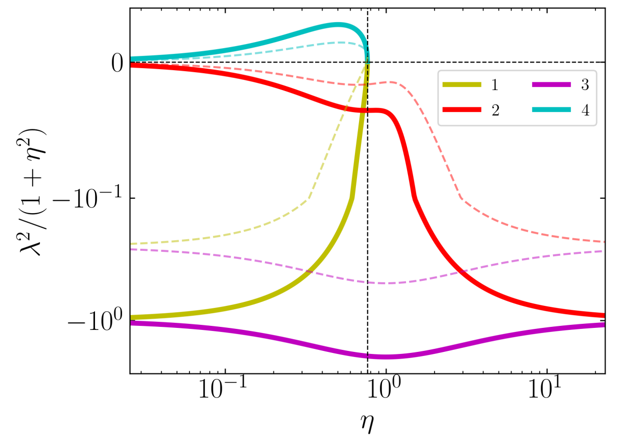

Figure 4. λ_0^2 (Eq. 17) as a function of $\eta \equiv |g|/\alpha$ for the four CSs. The solid lines give λ_0^2 for the unperturbed $\phi_{\rm cs}$, and the dashed lines give the values for $\phi_{\rm cs}$ shifted by 60° ($\phi_{\rm cs} = 120°$ for CS2 and $\phi_{\rm cs} = 60°$ for CSs 1, 3, and 4).

about each of the CSs in the presence of the weak tidal alignment torque. We can linearize Eqs. (11–12) about a shifted CS, yelding

$$\frac{\mathrm{d}}{\mathrm{d}t}\begin{bmatrix}\theta\\ \phi\end{bmatrix} = \begin{bmatrix} -\frac{\cos\theta}{t_{\rm s}} & -g\sin I\cos\phi \\ \alpha\sin\theta + g\frac{\sin I\cos\phi}{\sin^2\theta} & 0\end{bmatrix}_{\rm cs}\begin{bmatrix}\Delta\theta\\ \Delta\phi\end{bmatrix}, \tag{15}$$

where the cs subscript indicates evaluating at a CS, $\Delta\theta = \theta - \theta_{\rm cs}$, and $\Delta\phi = \phi - \phi_{\rm cs}$. The eigenvalues λ of Eq. (15) satisfy the equation

$$0 = \left(\lambda + \frac{\cos\theta_{\rm cs}}{t_{\rm s}}\right)\lambda - \lambda_0^2, \tag{16}$$

$$\lambda_0^2 \equiv \left(\alpha\sin\theta_{\rm cs} + g\sin I\csc^2\theta_{\rm cs}\cos\phi_{\rm cs}\right)\left(-g\sin I\cos\phi_{\rm cs}\right), \tag{17}$$

$$\lambda \approx -\frac{\cos\theta_{\rm cs}}{t_{\rm s}} \pm \sqrt{\lambda_0^2}. \tag{18}$$

The stability depends only on the real part of λ in Eq. (18). λ_0^2 is a generalization of Eq. (A4) in, Su & Lai (2020) and generally has the same behavior: it is negative for CSs 1–3 and positive for CS4, as shown in Fig. 4. Thus, CS4 is always unstable, as there will always be at least one positive solution for λ, and the stability of CSs 1–3 are solely determined by the sign of $\cos\theta_{\rm cs}$. From Figs. 1, we thus see that CSs 1 and 2 are stable while CS3 is unstable under the alignment torque. These calculations justify results long used in CS literature (e.g. Ward 1975).

3.2 Spin Obliquity Evolution Driven by Alignment Torque

With the above results, we are equipped to ask questions about the dynamics of Eqs. (11–12): what is the long term behavior for a general initial $\hat{\mathbf{s}}$? If $\eta > \eta_{\rm c}$, then the only possible final spin state is CS2, and all initial conditions will evolve asympotically towards it. As such, we consider only $\eta < \eta_{\rm c}$, where an initial condition can asymptotically evolve towards either CS1 or CS2. In Fig. 5, we show which CS an initial θ_0 and ϕ_0 evolves into, where we have taken $|g|\,t_{\rm s} = 10^{-3}$, $\eta = 0.2$, and $I = 20°$. It is clear that initial $\hat{\mathbf{s}}$ in zone

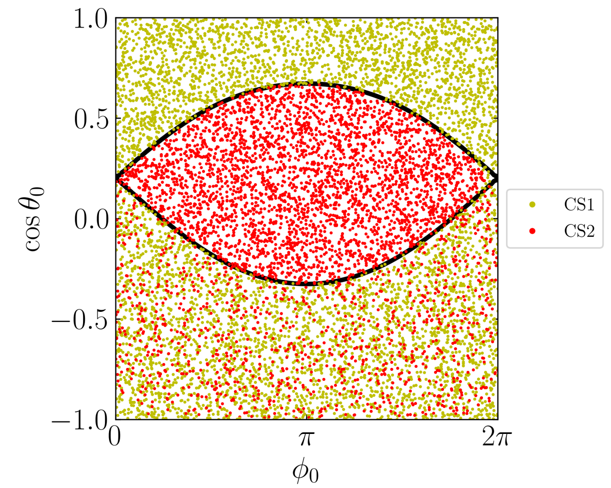

Figure 5. Plot illustrating the asymptotic behavior of initial conditions for $\eta = 0.2$ and $I = 20°$. Each dot represents an initial spin orientation, and the coloring of the dot indicates which Cassini State (legend) the system asymptotes towards.

I (following the naming in Fig. 2) evolve into CS1, those in zone II evolve into CS2, while those in zone III have a probabilistic outcome. We aim to understand each of these in turn:

For initial conditions in zone I, the spin circulates, and $\dot{\theta}$ is negative everywhere during the cycle. Thus, for initial conditions in zone I, θ decreases until the trajectory has converged to CS1. This is intuitively reasonable, as CS1 is stable.

For initial conditions in zone II, our stability calculation in Section 3.1 shows that initial conditions sufficiently near CS2 will converge to CS2. In fact, this result can be extended to all initial conditions inside the separatrix; see Appendix A.

For initial conditions in zone III, since there are no stable CSs in zone III, the system must evolve through the separatrix to reach one of either CS1 or CS2. The outcome of the separatrix encounter is effectively probabilistic and determines the final CS. Intuitively, this can be understood as probabilistic resonance capture: since $\eta \ll \eta_{\rm c}$, $\alpha \gg -g$ (the spin-orbit precession rate, Eq. 1, and the orbit precession induced by the perturber, Eq. 2, respectively), but $\alpha \cos\theta$ can become commensurate with $-g$ if $\cos\theta \sim \eta$. This is achieved as θ evolves from an initially retrograde obliquity through 90° towards 0° under the influence of the dissipative term in Eq. (11).

While similar in behavior to previous studies of probabilistic resonance capture (Henrard 1982; Su & Lai 2020), the underlying mechanism is different: in these previous studies, the phase space structure itself evolves and causes systems to transition among phase space zones, while in the present scenario, a non-Hamiltonian, dissipative perturbation causes systems to transition among unchanging phase space zones.

3.2.1 *Analytical Calculation of Resonance Capture Probability*

The specific probabilities of the two outcomes upon separatrix encounter, a zone III-II or a zone III-I transition, can be calculated analytically. Figure 6 shows how the perturbative alignment torque generates probabilistic outcomes upon separatrix encounter. We present the interpretation of Figure 6 and the calculation of the resonance capture probability by first giving a qualitative description of the intuition behind the method, then presenting a calculation in good agreement with numerical results.

We first describe the origin of the boundaries between regions of phase space that shown in Fig. 6. They are calculated numerically by integrating a point infinitesimally close to CS4 forward and backward in time. In the absence of the alignment torque, these trajectories would evolve along the separatrix, but in the presence of the alignment torque they are perturbed slightly and cease to overlap. It can be seen in Fig. 6 that this splitting opens a path from zone III into both zones I and II.

To understand this process quantitatively, as well as associate probabilities to the two possible outcomes, it is important to be more quantitative. The correct approach is to consider the evolution of the value of the *unperturbed* Hamiltonian (Eq. 9) as the spin evolves with the alignment torque. A point in zone III evolves such that H is increasing until $H \approx H_{\rm sep}$ where $H_{\rm sep}$ is the value of H along the separatrix, given by

$$\begin{aligned} H_{\rm sep} &\equiv H\left(\cos\theta_4, \phi_4\right), \\ &\approx -\alpha \sin I - g\cos^2 I + O\left(\eta^2\right), \end{aligned} \tag{19}$$

where θ_4 and ϕ_4 are the coordinates of CS4. As the system evolves closer to the separatrix, the change in H over each circulation cycle can be approximated by ΔH_-, the change in H along C_- (see Fig. 2). In general, we can compute $\Delta H_\pm$ the change over both legs of the separatrix with

$$\Delta H_\pm \equiv \oint\limits_{C_\pm} \frac{\mathrm{d}H}{\mathrm{d}t}\,\mathrm{d}t. \tag{20}$$

This can be simplified by using:

$$\begin{aligned} \frac{\mathrm{d}H}{\mathrm{d}t} &= \frac{\partial H}{\partial(\cos\theta)}\frac{\mathrm{d}(\cos\theta)}{\mathrm{d}t} + \frac{\partial H}{\partial\phi}\frac{\mathrm{d}\phi}{\mathrm{d}t}, \\ &= \left(\frac{\mathrm{d}(\cos\theta)}{\mathrm{d}t}\right)_{\rm tide}\frac{\mathrm{d}\phi}{\mathrm{d}t}, \end{aligned} \tag{21}$$

$$\Delta H_\pm = \mp\frac{1}{t_{\rm s}}\int\limits_0^{2\pi} \sin^2\theta\,\mathrm{d}\phi. \tag{22}$$

Thus, if we evaluate H every time that a trajectory crosses $\phi = 0$, we see that it will initially be negative and increase for each circulation cycle until the system encounters the separatrix where $H - H_{\rm sep} < \Delta H_-$.

When the system begins its separatrix-crossing orbit, H at $\phi = 0$ is in the range $\left[H_{\rm sep} - \Delta H_-, H_{\rm sep}\right]$; call this value $H_{\rm i}$, as it is the initial value of the Hamiltonian on the separatrix-crossing orbit. The two endpoints of this range are denoted in Fig. 8 by the black dot and cross at the left and right edges of the plot. Upon entering this range, the trajectory encounters the separatrix, and first traverses the vicinity of C_- then of C_+, after which two possible outcomes can occur:

- If the final value of H at the end of this separatrix traversal, denoted $H_{\rm f}$, satisfies $H_{\rm f} > H_{\rm sep}$, then the trajectory enters the separatrix, following the red shaded region in Fig. 8, and executes a zone III → II transition.
- If $H_{\rm f} < H_{\rm sep}$, then the trajectory exits the separatrix above CS4, following the yellow shaded region in Fig. 8 and executes a zone III → I transition.

Since $H_{\rm f} = H_{\rm i} + \Delta H_+ + \Delta H_-$, we find that if $H_{\rm i}$ is in the interval $\left[H_{\rm sep} - \Delta H_-, H_{\rm sep} - \Delta H_- - \Delta H_+\right]$, then the system executes a III → I transition, and if it is in the interval $\left[H_{\rm sep} - \Delta H_- - \Delta H_+, H_{\rm sep}\right]$, then the system executes a III → II transition. The values of $\cos\theta$ for which H is equal to $H_{\rm sep} - \Delta H_-$, $H_{\rm sep} - \Delta H_- - \Delta H_+$, and $H_{\rm sep}$ (CS4) for $\phi = 0$ are shown in Fig. 8 as the black cross, star, and dot at $\phi = 0$ respectively. Finally, if the alignment torque is weak, then $\Delta H_- \sim O\left(t_{\rm s}^{-1}\right)$ is small compared to the characteristic values of H, and $H_{\rm i}$ can be effectively considered as uniformly distributed over $\left[H_{\rm sep} - \Delta H_-, H_{\rm sep}\right]$. As such, we obtain that

$$P_{\rm III\to II} = \frac{\Delta H_- + \Delta H_+}{\Delta H_-}. \tag{23}$$

To actually evaluate Eq. (23), we use the parameterization for the separatrix (Su & Lai 2020) for $\eta \ll 1$:

$$(\cos\theta)_{C_\pm} \approx \eta\cos I \pm \sqrt{2\eta\sin I\left(1 - \cos\phi\right)}. \tag{24}$$

It can then be shown that

$$\Delta H_- \approx \frac{2\pi}{t_{\rm s}} + O(\eta), \tag{25}$$

$$\Delta H_+ + \Delta H_- \approx \frac{32\eta^{3/2}\cos I\sqrt{\sin I}}{t_{\rm s}}, \tag{26}$$

$$P_{\rm III\to II} \approx \frac{16\eta^{3/2}\cos I\sqrt{\sin I}}{\pi}. \tag{27}$$

Figure 7 displays the agreement of Eq. (27) with direct numerical simulations of Eqs. (5, 10), where good agreement is observed.

Finally, we remark that the calculation above is just a more descriptive application of *Melnikov's Method* (Guckenheimer & Holmes 1983). Melnikov's Method is a general integral that gives the degree of splitting of a "homoclinic orbit" (here, the separatrix) induced by a small, possibly periodic, perturbation. The explicit connection between the evolution of the unperturbed Hamiltonian and distances between curves in phase space (as depicted in Fig. 8) is provided by Melnikov's Method.

4 SPIN EVOLUTION WITH WEAK TIDAL FRICTION

4.1 Tidal Model: Equilibrium Tides

To model the dissipative effect of times, we use the weak friction theory of equilibrium tides (Lai 2012). In this model, tides cause

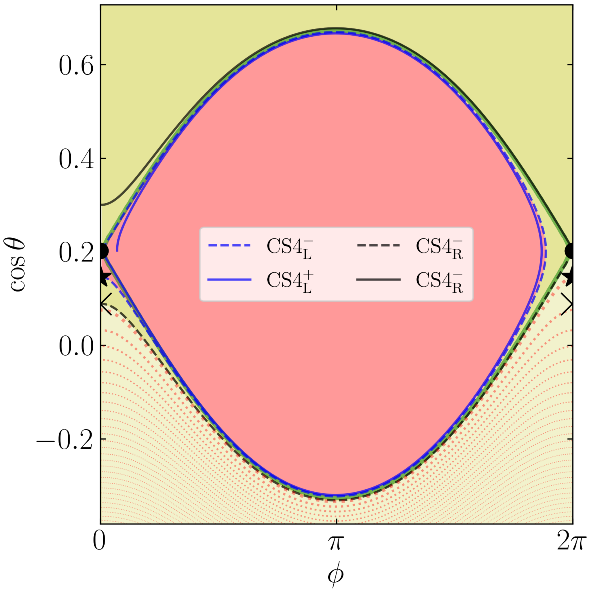

Figure 6. Plot illustrating the probabilistic origin of separatrix capture for $\eta = 0.2$ and $|g t_\mathrm{s}| = 10^3$. Yellow regions converge to CS1, and red to CS2. The separatrix of the unperturbed system is shown as the green line and splits due to the perturbative torque. To calculate the boundaries (legend) separating the CS1 and CS2-approaching regions, points near either the left or right copy of CS4 (L/R subscript) are evolved either forwards or backwards (± superscript). Within zone III, the regions of phase space reaching CS1 and CS2 both become very thin (shown qualitatively as the red dotted lines of decreasing width), reflecting the fact that the outcome for a particular initial condition can be approximated as probabilistic sufficiently far from the separatrix. Labeled in the black cross, star, and dot at the left and right edges of the plot are where H is equal to $H_\mathrm{sep} - \Delta H_-$, $H_\mathrm{sep} - \Delta H_- - \Delta H_+$, and H_sep (Eqs. 19 and 20).

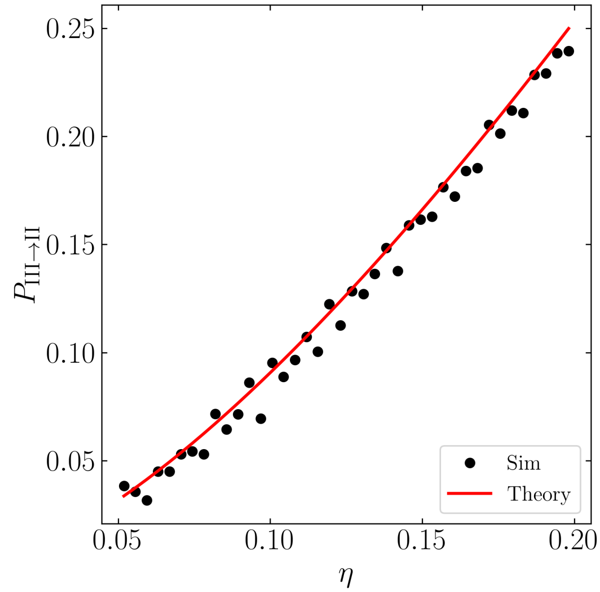

Figure 7. Plot of $P_{\mathrm{III}\to\mathrm{II}}$ as a function of η for the toy model. For each η, 150 initial θ_0 in zone III are evolved until separatrix encounter, where their outcome is recorded. Shown in red is Eq. (27).

both $\hat{\mathbf{s}}$ and Ω_s to evolve on the characteristic tidal timescale t_a:

$$\left(\frac{\mathrm{d}\hat{\mathbf{s}}}{\mathrm{d}t}\right)_\mathrm{tide} = \frac{1}{t_\mathrm{a}}\left[\frac{2n}{\Omega_\mathrm{s}} - \left(\hat{\mathbf{s}}\cdot\hat{\mathbf{l}}\right)\right]\hat{\mathbf{s}}\times\left(\hat{\mathbf{l}}\times\hat{\mathbf{s}}\right), \tag{28}$$

$$\frac{1}{\Omega_\mathrm{s}}\left(\frac{\mathrm{d}\Omega_\mathrm{s}}{\mathrm{d}t}\right)_\mathrm{tide} = \frac{1}{t_\mathrm{a}}\left[\frac{2n}{\Omega_\mathrm{s}}\left(\hat{\mathbf{s}}\cdot\hat{\mathbf{l}}\right) - 1 - \left(\hat{\mathbf{s}}\cdot\hat{\mathbf{l}}\right)^2\right], \tag{29}$$

where t_a is given by

$$\frac{1}{t_\mathrm{a}} \equiv -\frac{L}{2S}\frac{\Omega_\mathrm{s}}{2n}\frac{3k_2}{Q}\left(\frac{m}{M}\right)\left(\frac{R}{a}\right)^5 n. \tag{30}$$

Here, $L = ma^2 n$ and $S = kmR^2 \approx mR^2/4$ are the orbital and spin angular momenta of the inner planet, respectively. We neglect orbital evolution in this section since the time scale is longer than t_a by a factor of $\sim L/S \gg 1$, and so t_a is a constant. We will continue mostly consider the case where $|g t_\mathrm{a}| \gg 1$.

To understand the long-term behaviors of the system, we first consider its behavior near a CS. Specifically, we wish to understand whether initial conditions near a CS stay near the CS as the evolution of Ω_s causes the CSs to evolve. We first note that the evolution of Ω_s does not drive spins towards or away from CSs: as long as it evolves sufficiently slowly (adiabatically, Su & Lai 2020), conservation of phase space area ensures that trajectories will remain at a roughly fixed distance to stable equilibria of the system. Thus, Eq. (28) alone determines whether a point evolves towards or away from a nearby CS

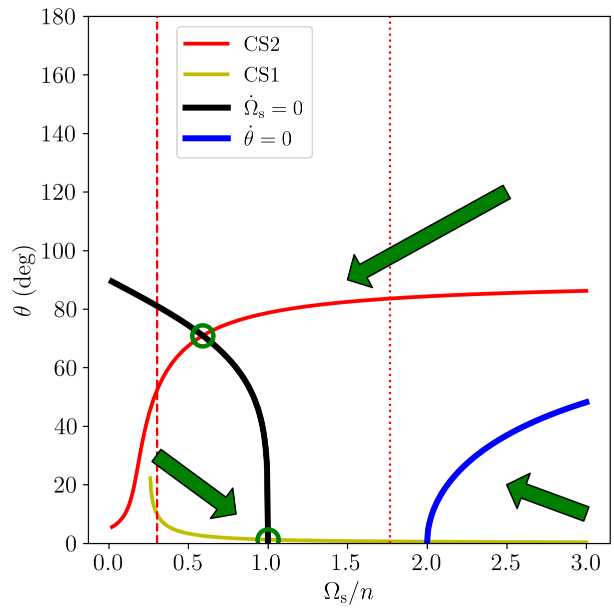

Figure 8. Schematic illustrating the evolution of the planet's spin due to tidal friction for $I = 5°$ and $\eta_\mathrm{sync} = 0.2$. The green lines illustrate the directions of Eqs. (28–29), while the black and blue lines denote where the tidal $\dot{\Omega}_\mathrm{s}$ and $\dot{\theta}$ change signs respectively. Overlaid are the obliquities of Cassini States 1 and 2, the two Cassini States that are stable under tidal dissipation (see Section 3.1). The points that are both Cassini States and satisfy $\dot{\Omega}_\mathrm{s} = 0$ are the tidal Cassini Equilibria (tCE), circled in green. Finally, the vertical red lines illustrate the Ω_s below which tides causes tCE2 to become unstable; the dashed and dotted vertical red lines lines correspond to values of $|g t_\mathrm{a}|^{-1} = 10^{-2}$ and 10^{-1} respectively.

as Ω_s evolves. Then, evaluating Eq. (18) with $t_s = t_a/(2n/\Omega_s - \cos\theta)$ (compare Eqs. 10 and Eq. (28)), we see that CS2 is still always stable, while CS1 is becomes unstable for $\Omega_s > 2n$.

Using this result, we can then identify the long-term equilibria of the system (i.e. when including the evolution of Ω_s), as the long-term equilibria of the system must both satisfy $\dot{\Omega}_s = 0$ and be a stable CS. Figure 8 shows the behavior of Eqs. (28–29) qualitatively in the coordinates (Ω_s, θ), along with the locations of CS1 and CS2. The two points circled in green in Fig. 8 satisfy the criteria to be long-term equilibria, and we call them *tidal Cassini Equilibria* (tCE). We number tCE1 and tCE2 the tCE that are in CSs 1 and 2 respectively.

There are two important caveats that may change the existence and stability of the tCE. First, if $\eta \geq \eta_c$ (Eq. (8)) when $\Omega_s \approx n$[1], then tCE1 will not exist. We can define the constant parameter

$$\eta_{\rm sync} \equiv \left(\eta\right)_{\Omega_s = n}, \tag{31}$$

where the existence of tCE1 then requires $\eta_{\rm sync} \leq \eta_c$. Secondly, tCE2 may not be stable if the tidal phase shift is too large, as discussed in Section 3.1. This threshold is shown as the vertical red lines in Fig. 8 for a few choices of t_a.

4.2 Spin Obliquity Evolution as a Function of Initial Spin Orientation

With this result, we can now consider the final fate of the inner planet's spin. We assume that the planet is initially rotating supersynchronously and adopt the fiducial initial spin frequency $\Omega_{s,i} = 10n$. The final results are not sensitive on the specific initial spin as long as $\Omega_{s,i} \gg n$. Then, for a given initial θ_0 and ϕ_0, the final outcome (either tCE1 and tCE2) of the system can be calculated by direct integration of Eqs. (5, 28–29). In Fig. 9, we show the final outcome for many randomly chosen θ_0 and ϕ_0 for $\eta_{\rm sync} = 0.06$ and $I = 5^\circ$. We see that tCE1 is generally reached for spins initially in zone I, tCE2 is generally reached for spins initially in zone II, and a probabilistic outcome is observed for spins initially in zone III, very similar to the results found for the toy model in Section 3. Figures 10 and 11 show the same results but for $\eta_{\rm sync} = 0.2$ and $\eta_{\rm sync} = 0.7$. As $\eta_{\rm sync}$ is increased, more initial conditions reach tCE2. This is both because there are more systems initially in zone II and because more systems initially in zone III execute a III $\rightarrow$ II transition upon separatrix encounter.

4.2.1 *Analytical Calculation of Resonance Capture Probability*

Even when including the evolution of Ω_s, and therefore the spin-orbit precession frequency α, the probabilities of the III $\rightarrow$ I and III $\rightarrow$ II transitions upon separatrix encounter can be computed. The calculation is more involved than that presented in Section 3.2, and also incorporates the seminal resonance capture theory of Henrard (1982). In the interest of clarity, we give an overview of the approach, and present the analytical results of the calculation in Appendix B.

In Section 3.2, we found that keeping track of the value of H, the value of the unperturbed Hamiltonian, allowed us to calculate the probabilities of the various outcomes of separatrix encounter. Specifically, the outcome upon separatrix encounter is determined by the value of H at the start of the separatrix-crossing orbit relative to $H_{\rm sep}$, the value of H along the separatrix. When the spin is also evolving, $H_{\rm sep}$ is also changing during the separatrix-crossing orbit,

[1] Strictly, if η is very close to η_c, the planet's spin is slightly subsynchronous at tCE1, see Fig. 8.

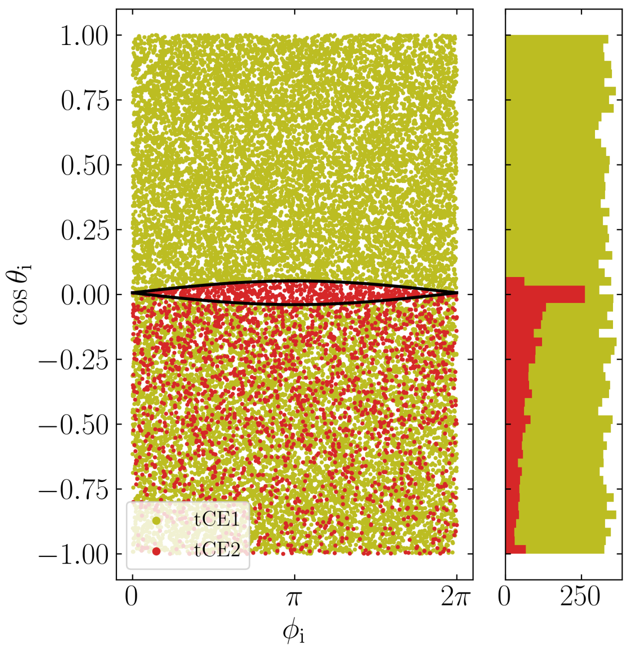

Figure 9. *Left:* Each dot indicates which tCE a given initial condition (θ_i, ϕ_i) evolve towards (labeled in legend), for $\eta_{\rm sync} = 0.06$ and $I = 5^\circ$. The separatrix is shown as the black line. Note that points above the separatrix evolve towards tCE1, points inside the separatrix evolve towards tCE2, and points below the separatrix have a probabilistic outcome. *Right:* Histogram of which tCE a given initial obliquity θ_i evolves towards.

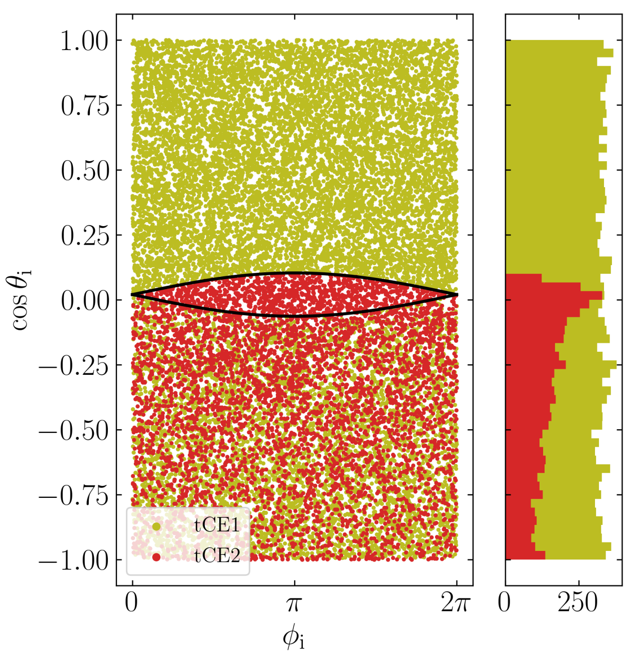

Figure 10. Same as Fig. 9 but for $\eta_{\rm sync} = 0.2$.

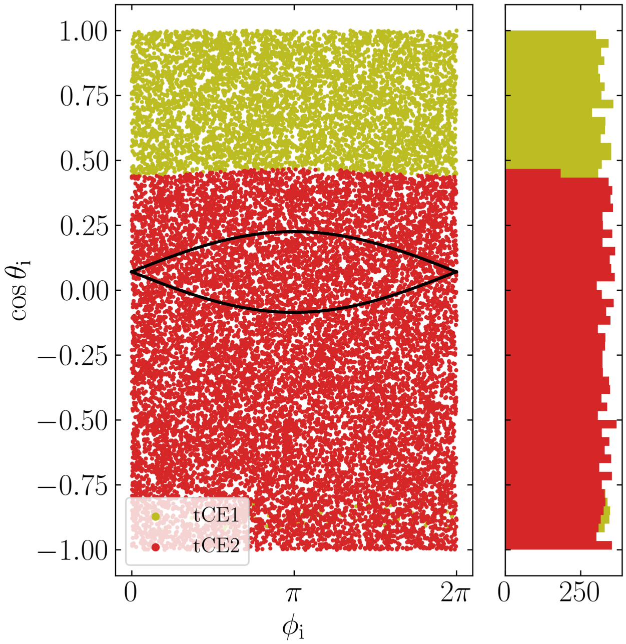

Figure 11. Same as Fig. 9 but for $\eta_{\rm sync} = 0.7$. Note that even points above the separatrix can evolve towards tCE2 here.

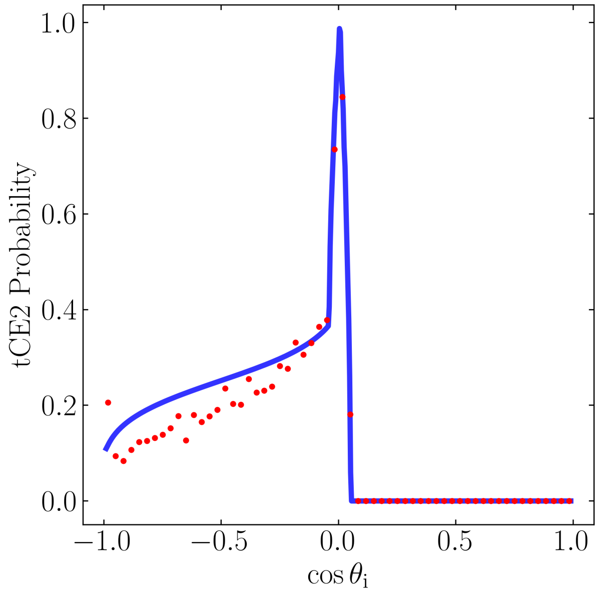

Figure 12. Comparison of the right hand panel of Fig. 9 (red dots) with a semi-analytic calculation (blue line). The semi-analytic calculation is performed by numerically integrating Eqs. (5, 28–29) on a grid of initial conditions uniform in $\cos\theta_{\rm i}$ and $\phi_{\rm i}$ until separatrix encounter, then using the $\Omega_{\rm s}$ at separatrix encounter to evaluate (TODO) to analytically compute the probability of evolution into tCE2.

and the discussion in Section 3.2 must be generalized to account for this. Instead of focusing on the evolution of H along a trajectory, we instead follow the evolution of

$$K \equiv H - H_{\rm sep}. \tag{32}$$

Note that $K > 0$ inside the separatrix, and $K < 0$ outside. Then, the outcome of the separatrix-crossing orbit is largely the same as discussed in Section 3.2. First, we must compute the change in K along the legs of the separatrix. We define $\Delta K_\pm$ by generalizing Eq. (20) very naturally:

$$\Delta K_\pm = \oint_{C_\pm} \frac{\mathrm{d}H}{\mathrm{d}t} - \frac{\mathrm{d}H_{\rm sep}}{\mathrm{d}t}\;\mathrm{d}t. \tag{33}$$

Here, however, note that $C_\pm$ depends on the value of $\Omega_{\rm s}$ upon separatrix encounter! Since there is no closed form solution for $\Omega_{\rm s}(t)$, the probabilities of the various outcomes can only be determined as a function of the system properties at separatrix encounter, and not as a simple function of the initial conditions.

Then, if we call K_i the value of K at the start ($\phi = 0$) of the separatrix-crossing orbit, $K_i > -\Delta K_+ - \Delta K_-$ gives a III $\to$ II transition and eventual evolution towards tCE2 while $-\Delta K_- < K_i < -\Delta K_- - \Delta K_+$ gives a III $\to$ I transition and ultimate evolution towards tCE1. Thus, we find that the probability of a III $\to$ II transition is given by

$$P_{\rm III\to II} = \frac{\Delta K_+ + \Delta K_-}{\Delta K_-}. \tag{34}$$

The analytical approximate forms for $\Delta K_\pm$ are given in by Eq. (B7). Note that Eqs. (33, 34) are equivalent to the separatrix capture result of Henrard (1982) when $\cos\theta$ is not evolving (Henrard & Murigande 1987). Here, we argue that this classic calculation can be unified with the calculation given in Section 3.2 to give an accurate prediction of separatrix encounter outcome probabilities in the presence of both a dissipative perturbation and a parametric variation of the Hamiltonian.

To compare Eq. (34) with numerical simulations, we can integrate Eqs. (5, 28–29) for many initial conditions in Zone III while evaluating $P_{\rm III\to II}$ (and thus also obtaining $P_{\rm III\to I} = 1 - P_{\rm III\to II}$) for each simulation at the moment it encounters the separatrix. If the theory is correct, the total numbers of systems converging to each of tCE1 and tCE2 should be equal to those predicted by the sums of the calculated probabilities. In Fig. 12, we show the agreement of this semi-analytic procedure with the numerical results displayed earlier in the right panel of Fig. 9. Good agreement is observed. Figs. 13 and 14 show the same for Figs. 10 and 11. Mostly satisfactory agreement is observed. Thus, we conclude that the outcomes of separatrix encounter are accurately predicted by Eq. (34).

4.3 Spin Obliquity Evolution as a Function of Precession Strength

In the previous section, we considered the outcome as a function of the initial spin orientation, specified by θ_0 and ϕ_0. In this section, we consider the distribution of outcomes when averaging over a distribution of initial spin orientations. For simplicity, we just consider $\hat{\mathbf{s}}$ being isotropically distributed. Figure 15 shows this for $I = 5^\circ$ as a function of $\eta_{\rm sync}$. where ϵ is the dimensionless tidal evolution rate,

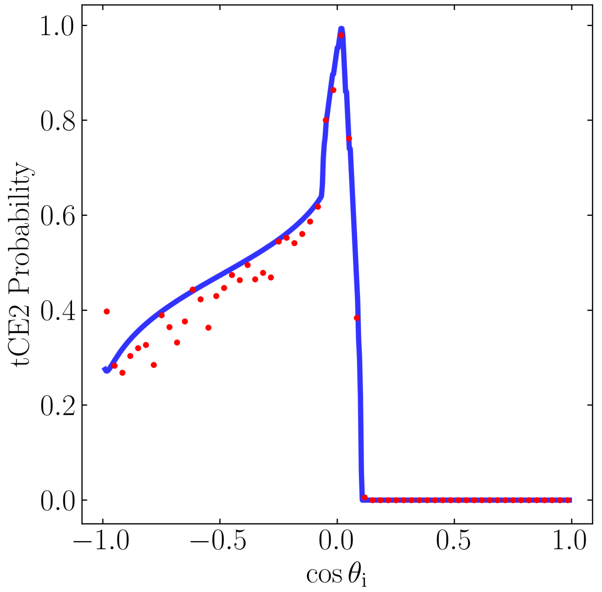

Figure 13. Same as Fig. 12 but for $Omega_{\rm c} = 0.2$, shown in Fig. 10.

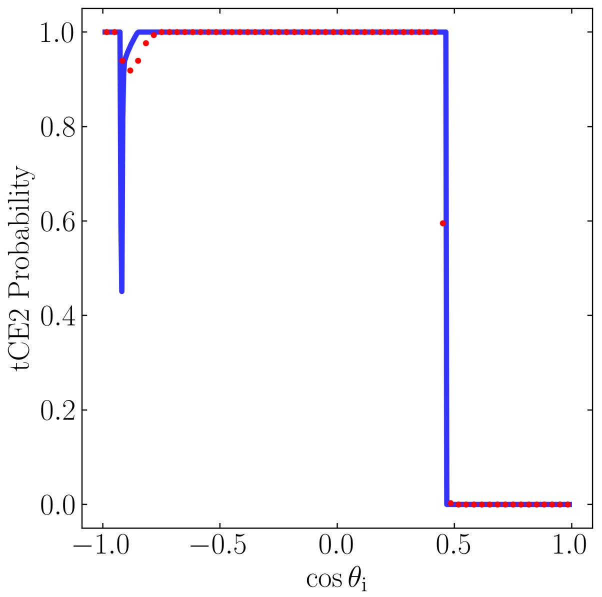

Figure 14. Same as Fig. 12 but for $\eta_{\rm sync} = 0.7$, shown in Fig. 11.

given by

$$\epsilon \equiv -\frac{1}{gt_a}\frac{L}{2S}\frac{\Omega_{\rm s}}{2n}, \tag{35}$$

$$\frac{1}{t_a} = \frac{3k_2}{Q}\left(\frac{m}{M}\right)\left(\frac{R}{a}\right)^5 n, \tag{36}$$

$$\epsilon \approx 0.003\frac{1}{\cos I}\left(\frac{2k_2/Q}{10^{-3}}\right)\left(\frac{m_{\rm p}}{M_{\rm J}}\right)^{-1}\left(\frac{a_{\rm p}}{5\ {\rm AU}}\right)^3 \times\left(\frac{a}{0.4\ {\rm AU}}\right)^{-6}\left(\frac{\rho}{3\ {\rm g/cm^3}}\right)^{-1}\left(\frac{M_\star}{M_\odot}\right)^2. \tag{37}$$

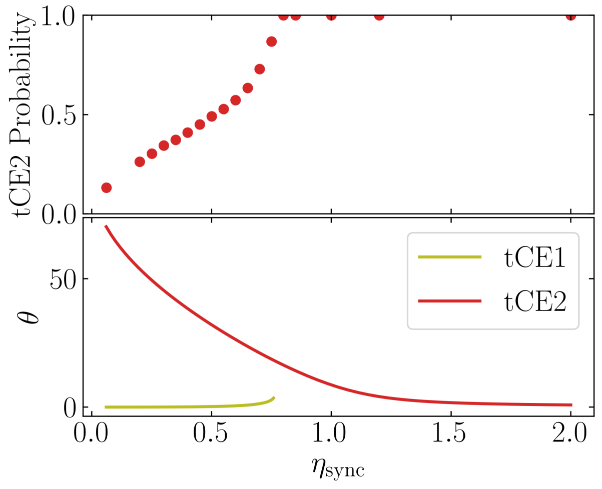

Figure 15. *Top:* Total probability of ending up in tCE2 (red dots) for $I = 5°$ for a range of $\eta_{\rm sync}$. *Bottom:* obliquities of the two possible tCE.

5 APPLICATIONS

5.1 Application to SE+HJ Systems

Consider a system consisting of an inner Super-Earth (SE) and an exterior cold Jupiter (CJ). For this system, Eq. (31) can be evaluated

$$\eta_{\rm sync} = 0.33\left(\frac{k}{k_{\rm q}}\right)\left(\frac{m_{\rm p}}{M_{\rm J}}\right)\left(\frac{a_{\rm p}}{5\ {\rm AU}}\right)^{-3} \times\left(\frac{a}{0.4\ {\rm AU}}\right)^6\left(\frac{\rho}{3\ {\rm g/cm^3}}\right)\left(\frac{M_\star}{M_\odot}\right)^{-2}. \tag{38}$$

Here, $\rho = m/\left(4\pi R^3/3\right)$ is the average density of the inner planet, and $M_{\rm J}$ is the mass of Jupiter. Tides tend to drive $\Omega_{\rm s}$ to spin-orbit synchronization, where $\Omega_{\rm s} = n$ and thus $-g/\alpha = \Omega_{\rm c}/n$. As such, we see that the ratio $\Omega_{\rm c}/n$ quantifies the strength of the perturber relative to the spin-orbit coupling at the tidal equilibrium.

6 SUMMARY AND DISCUSSION

REFERENCES

Anderson, K. R., & Lai, D. 2018, Monthly Notices of the Royal Astronomical Society, 480, 1402

Colombo, G. 1966, SAO Special Report, 203

Fabrycky, D. C., Johnson, E. T., & Goodman, J. 2007, The Astrophysical Journal, 665, 754

Guckenheimer, J., & Holmes, P. J. 1983, Nonlinear oscillations, dynamical systems, and bifurcations of vector fields (New York: Springer-Verlag)

Henrard, J. 1982, Celestial Mechanics and Dynamical Astronomy, 27, 3

Henrard, J., & Murigande, C. 1987, Celestial Mechanics, 40, 345

Lai, D. 2012, Monthly Notices of the Royal Astronomical Society, 423, 486

Lainey, V. 2016, Celestial Mechanics and Dynamical Astronomy, 126, 145

Millholland, S., & Batygin, K. 2019, The Astrophysical Journal, 876, 119

Peale, S. J. 1969, The Astronomical Journal, 74, 483

Su, Y., & Lai, D. 2020, arXiv preprint arXiv:2004.14380

Ward, W. R. 1975, The Astronomical Journal, 80, 64

APPENDIX A: CONVERGENCE OF INITIAL CONDITIONS INSIDE THE SEPARATRIX TO CS2

In Section 3.1, we studied the stability of the CSs under of tidal alignment torque given by Eq. (10), finding that CS2 is locally stable. Later, in Section 3.2, we found that all initial conditions within the separatrix converge to CS2, which is not guaranteed by local stability of CS2. In this section, we give an analytic demonstration that all points inside the separatrix indeed converge to CS2, focusing on the case where $\eta \ll 1$.

Similarly to the analytic calculation in Section 3.2, we seek to compute the change in the unperturbed Hamiltonian over a single libration cycle. To calculate the evolution of H, we first parameterize the unperturbed trajectory (similarly to Eq. 24). For initial conditions inside the separatrix, the value of H can be written $H = H_{\rm sep} + \Delta H$ where $\Delta H > 0$, and the two legs of the libration trajectory can be written:

$$\cos\theta_{\pm} \approx \eta\cos I \pm \sqrt{2\eta\left[\sin I\left(1 - \cos\phi\right) - \Delta H\right]}. \tag{A1}$$

We have taken $\sin\theta \approx 1$, a good approximation in zone II since $\eta \ll 1$. Note that there are some values of ϕ for which no solutions of θ exist, reflecting the fact that the libration cycle does not extend over the full interval $\phi \in [0, 2\pi]$. During a libration cycle, θ_- $[\theta_+]$ is traversed while $\phi' > 0$ $[\phi' < 0]$, i.e. the trajectory librates counterclockwise in $(\cos\theta, \phi)$ phase space (see Fig. 2).

The leading order change to H over a single libration cycle can then computed by integrating $\mathrm{d}H/\mathrm{d}t$ along this trajectory, yielding:

$$\begin{aligned}\oint \frac{\mathrm{d}H}{\mathrm{d}t}\,\mathrm{d}t &= \oint \left(\frac{\mathrm{d}(\cos\theta)}{\mathrm{d}t}\right)_{\rm tide}\,\mathrm{d}\phi,\\ &= \int\limits_{\phi_{\min}}^{\phi_{\max}} \frac{1}{t_{\rm s}}\left(\sin^2\theta_- - \sin^2\theta_+\right)\,\mathrm{d}\phi\\ &= \frac{1}{t_{\rm s}}\int\limits_{\phi_{\min}}^{\phi_{\max}} 4\eta\cos I\sqrt{2\eta\left[\sin I\left(1-\cos\phi\right) - \Delta H\right]}\,\mathrm{d}\phi > 0.\end{aligned} \tag{A2}$$

Here, $\phi_{\min} > 0$ and $\phi_{\max} < 2\pi$ are defined such that the trajectory librates over $\phi \in [\phi_{\min}, \phi_{\max}]$. Thus, H is strictly increasing for all initial conditions inside the separatrix, and they all converge to CS2.

APPENDIX B: SEPARATRIX CROSSING PROBABILITY WITH WEAK TIDAL FRICTION

In this appendix, we analytically calculate $\Delta K_{\pm}$ for use in Eq. (34) to calculate the probabilities of the two possible transitions upon separatrix encounter. We first rewrite the full equations of motion for the planet's spin including weak tidal friction in component form:

$$\frac{\mathrm{d}\theta}{\mathrm{d}t} = g\sin I\sin\phi - \frac{1}{t_{\rm a}}\sin\theta, \tag{B1}$$

$$\frac{\mathrm{d}\phi}{\mathrm{d}t} = -\alpha\cos\theta - g\left(\cos I + \sin I\cot\theta\cos\phi\right), \tag{B2}$$

$$\frac{\mathrm{d}\Omega_{\rm s}}{\mathrm{d}t} = \frac{1}{t_{\rm a}}\left[2n\cos\theta - g\Omega_{\rm s}\left(1 + \cos^2\theta\right)\right]. \tag{B3}$$

Note that Eq. (33) can be rewritten

$$\begin{aligned}\Delta K_{\pm} &= \oint_{C_\pm} \frac{\mathrm{d}H}{\mathrm{d}t} - \frac{\mathrm{d}H_{\rm sep}}{\mathrm{d}t}\,\mathrm{d}t\\ &= \oint_{C_\pm}\left(\frac{\mathrm{d}(\cos\theta)}{\mathrm{d}t}\right)_{\rm tide} + \frac{\dot{\Omega}_{\rm s}}{\dot{\phi}}\left(\frac{\partial H}{\partial s} - \frac{\partial H_{\rm sep}}{\partial s}\right)\,\mathrm{d}\phi.\end{aligned} \tag{B4}$$

We then evaluate $\Delta K_{\pm}$ by integrating along the separatrix, using the parameterized form for $(\cos\theta)_{C_\pm}$ given by Eq. (24). Note that we must use the value of η at the moment of separatrix encounter, as the evolution of $\Omega_{\rm s}$ changes the spin-orbit precession frequency α NB: I haven't analytically recalculated this formula recently, only compared numerically, so there may be small typos, though nothing that changes the accuracy of the result:

$$\Delta K_{\pm} = \oint_{C_\pm} \frac{1}{t_{\rm s}}\sin^2\theta\left(\frac{2n}{\Omega_{\rm s}} - \cos\theta\right) + \left[\alpha\frac{\cos^2\theta}{2} + g\frac{\Omega_{\rm c}}{2\Omega_{\rm s}^2}\cos^2 I\right]\frac{\mathrm{d}\Omega_{\rm s}}{\mathrm{d}t}\frac{\mathrm{d}t}{\mathrm{d}\phi}\,\mathrm{d}\phi \tag{B5}$$

$$\approx \oint_{C_\pm}\frac{1}{t_{\rm s}}\sin^2\theta\left(\frac{2n}{\Omega_{\rm s}} - \cos\theta\right) + \frac{1}{t_{\rm s}}\frac{n}{\Omega_{\rm s}\eta}\left[(\cos\theta)_{C_\pm} - \frac{\Omega_{\rm s}}{2n}\right]\left[2\cos I \pm \sqrt{2\sin I\left(1-\cos\phi\right)/\eta}\right]\,\mathrm{d}\phi, \tag{B6}$$

$$\begin{aligned}t_{\rm s}\Delta K_{\pm} \approx{}& -2\cos I\left(\pm 2\pi\eta\cos I + 8\sqrt{\eta\sin I}\right) \pm 2\pi\frac{\Omega_{\rm s}}{n}\cos I - 8\eta\cos I\sqrt{\sin I/\eta} + \frac{4\Omega_{\rm s}}{n}\sqrt{\sin I/\eta}\\ &+ \frac{2n}{\Omega_{\rm s}}\left(\mp 2\pi\left(1 - 2\eta\sin I\right) + 16\cos I\eta^{3/2}\sqrt{\sin I}\right) + 8\sqrt{\eta\sin I} \pm 2\pi\eta\cos I - \frac{64}{3}\left(\eta\sin I\right)^{3/2}.\end{aligned} \tag{B7}$$

This is used in Eq. (34) to semi-analytically compute the tCE2 probabilities (blue curves) in Figs. 12–14.